Full Paper

Israel Journal of Chemistry

DOI: 10.1002/ijch.202000009

Catalytically Active Iron(IV)oxo Species Based on a Bis(pyridinyl)phenanthrolinylmethane

Henrika M. Hüppe,[a] Kristina Keisers,[a] Fabian Fink,[a] Sonja D. Mürtz,[a] Alexander Hoffmann,[a] Linda Iffland,[b] Ulf-Peter Apfel,[b, c] and Sonja Herres-Pawlis*[a]

Dedicated to Prof. Sason Shaik

Abstract: Starting from the mononuclear iron(II) complex $[Fe(MeCPy_2Phen)(MeCN)_2]^{2+}$, a non-heme Fe(IV)oxo complex $[Fe^{IV}(MeCPy_2Phen)O]^{2+}$ was synthesized via oxidation with *meta*-chloroperoxybenzoic acid (mCPBA). The Fe(IV)oxo complex was characterized using UV/Vis spectroscopy, Mößbauer spectroscopy and CSI mass spectrometry. The ability of this species to oxidize C–H bonds was tested with cyclohexane and adamantane as model substrates. For cyclohexane, an alcohol-to-ketone ratio (*A*/*K*) of 6.1 and efficiencies up to 55 were obtained. In case of adamantane, the ratio of tertiary over secondary products (3°/2°) is 38. In combination, this indicates the iron(IV)oxo complex being the catalytically active species.

Keywords: Iron · Bioinorganic Chemistry · C–H activation · N ligands · Oxidation

1. Introduction

High-valent iron-oxo species are a common motive for the active species in natural enzymes and catalyze a plethora of difficult oxidative functionalization reactions.[1] This includes olefin cis-dihydroxylation, olefin epoxidation and C–H bond oxidation.[2] An example for the first-mentioned reaction is mediated by the iron-containing Rieske dioxygenase, a non-heme iron species.[3] The last two reactions can be performed by either heme enzymes like cytochrome P450[4] or non-heme ones like methane monooxygenase.[5]

The oxidation of C–H bonds is of great interest due to the thermodynamic stability and kinetic inertness of this bond and the large variety of hydrocarbon feed stocks available in chemistry.[6] It is not surprising that in the last decades many chemists made efforts towards mimicking the properties of these enzymes with high-valent iron-oxo complexes.[1,7–10] Especially the mild reaction conditions as well as the efficiency and selectivity of the natural paragons are worth recreating their reactivities.[7,11] Additionally, iron is the fourth most abundant metal in the earth crust.[12] This makes iron a good candidate as cheap and moreover non-toxic metal for transition metal catalysis.[7,8]

It is possible to synthesize non-heme iron-oxo complexes with a wide range of tetra- and pentadentate ligands.[7] The first crystal structure of a non-heme Fe(IV) oxo model complex was obtained in 2003 with the tetradentate ligand 1,4,8,11-tetramethyl-1,4,8,11-tetraazacyclotetradecane (TMC).[13] Beforehand, around the millennium turn, first landmark studies regarding catalytic alkane hydroxylation with high-valent iron-oxo species were undertaken.[8,14] A ligand used for this studies was e. g. the tetradentate tris-pyridinylligand TPA (see. Scheme 1, A)). The first tetradentate Fe(IV)oxo complex identified by several spectroscopic methods was $[Fe(IV)(O)(TPA)(MeCN)]^{2+}$.[9,15] On the one hand, Fe(IV)oxo complexes with tetradentate ligands are less stable than those with pentadentate ligands.[9] On the other hand, complexes with tetradentate ligands offer the possibility of having a *cis*-labile coordination site in the iron(II) precursor complex different than the pentadentate ligand-based precursor complexes. For some of the proposed reaction mechanisms it seems to be key, that there are two *cis*-labile coordination sites for the oxidation of the metal center and the subsequent selective substrate oxidation reaction.[6,8] Se-

[a] *H. M. Hüppe, K. Keisers, F. Fink, S. D. Mürtz, Dr. A. Hoffmann, Prof. Dr. S. Herres-Pawlis*
Institute of Inorganic Chemistry, RWTH Aachen University
Landoltweg 1a, 52074 Aachen, Germany
phone: +49 241 80 93903
fax: +49 241 80 92074
E-mail: sonja.herres-pawlis@ac.rwth-aachen.de
[b] *L. Iffland, Prof. Dr. U.-P. Apfel*
Inorganic Chemistry I, Ruhr-Universität Bochum
Universitätsstraße 150, 44801 Bochum, Germany
[c] *Prof. Dr. U.-P. Apfel*
Fraunhofer UMSICHT
Osterfelder Straße 3, 46047 Oberhausen, Germany

Supporting information for this article is available on the WWW under https://doi.org/10.1002/ijch.202000009

© 2020 The Authors. Published by Wiley-VCH Verlag GmbH & Co. KGaA. This is an open access article under the terms of the Creative Commons Attribution Non-Commercial NoDerivs License, which permits use and distribution in any medium, provided the original work is properly cited, the use is non-commercial and no modifications or adaptations are made.

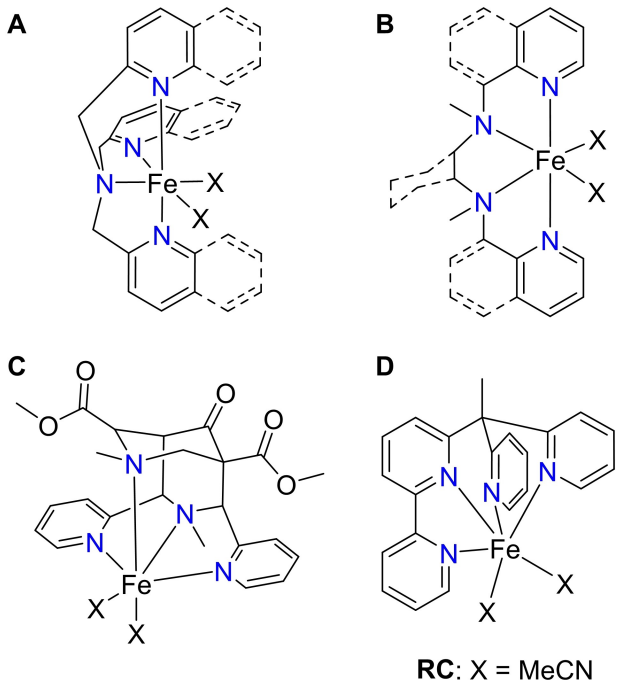

Scheme 1. Literature examples of iron(II) precursor complexes with *cis*-labile coordination site for Fe(IV)oxo species. Ligands shown are: A) tris(2-pyridylmethyl)amine (TPA)[15] /tris(2-quinolylmethyl)amine (TQA)[16]; B) *N,N'*-dimethyl-*N,N'*-bis(8-quinolyl)ethane-1,2-diamine (BQEN)[17] /L *N,N'*-dimethyl-*N,N'*-bis(8-quinolyl)cyclohexanediamine (BQCN)[18] /*N,N'*-bis(2-pyridylmethyl)-*N,N'*-dimethyl-*trans*-1,2-diaminocyclohexane (BPMCN)[19]; C) 3,7-dimethyl-2,4-bis(pyridin-2-yl)-9-oxo-3,7-diazabicyclo[3.3.1]nonane-1,5-dicarboxylic acid dimethyl ester, (a bispidine ligand)[20]; D) 6-(1,1-di(pyridine-2-yl)ethyl)-2,2'-bipyridine ($MeCPy_2BiPy$).[6]

lected literature examples of such ligands are shown in Scheme 1. All of the ligands have pyridinyl(-like) donors, in case of A–C combined with amines. The tripodal ligands of A) are TPA[15] and TQA with one central amine and three pyrininyl(-like) donors.[16] In contrast to compound class A), the ligands of B) BQEN,[17] BQCN[18] and BPMCN[19] as well as C) a bispidine ligand[20] have only two pyridinyl (-like) donors and two amine donors. An example for a ligand with only pyridinyl(-like) donors is 6-(1,1-di (pyridine-2-yl)ethyl)-2,2'-bipyridine ($MeCPy_2BiPy$)[6] in D). With all these complexes it is possible to obtain an Fe(IV) oxo species.

Herein, we report the syntheses of the tetradentate ligand $MeCPy_2Phen$ (**L**) and two associated iron(II) complexes [Fe ($MeCPy_2Phen$)$(MeCN)_2$](OTf)$_2$ (**C1**) and [Fe($MeCPy_2Phen$) $(MeCN)_2$]$(BF_4)_2$ (**C2**) (where $MeCPy_2Phen$ is 2-(1,1-di (pyridin-2-yl)ethyl)-1,10-phenanthroline and OTf is triflate). **L** is in terms of structure similar to the literature known ligand $MeCPy_2BiPy$.[6] Both provide two pyridinyl donor moieties. We highlight the phenanthrolinyl unit in contrast to the bipyridinyl unit of the literature known ligand. Although phenanthroline is a weaker donor than the closely related BiPy,[21] it provides a higher degree of preorganization and coordinative stability due to the more rigid backbone. We propose that this should lead to larger TONs in oxidative since the iron coordination is more stable and thus fosters regeneration of the catalytically active species.

2. Results and Discussion

2.1 Synthesis and Characterization of the Iron(II) Complexes

L can be obtained from 2,2'-(ethane-1,1-diyl)dipyridine by deprotonation with *n*BuLi and subsequent nucleophilic substitution with 2-bromo-1,10-phenanthroline (Scheme 2).

In addition to the standard characterization via NMR spectroscopy and EI mass spectrometry, single crystals suitable for X-ray diffraction could be obtained. **L** crystallizes in the triclinic space group $P\bar{1}$ with two ligand molecules in the asymmetric unit (**L** and **L'**) (Figure 1). As listed in Table 1 the values for bond lengths and angles around the apical carbon of the two independent molecules are equal. The largest difference can be seen in the torsion of the phenanthrolinyl residue represented by the dihedral angle N_{Phen}–C–C–N_{Phen} which is contrary to each other (**L**: 2.5(2) vs. **L'**: −5.2(3) °).

The iron(II) complexes [Fe($MeCPy_2Phen$)$(MeCN)_2$](OTf)$_2$ (**C1**) and [Fe($MeCPy_2Phen$)$(MeCN)_2$]$(BF_4)_2$ (**C2**) can be

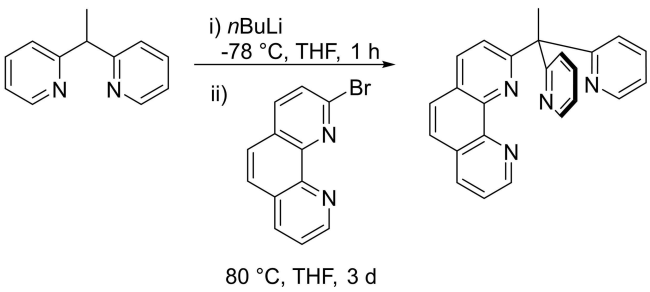

Scheme 2. Synthesis of ligand **L**.

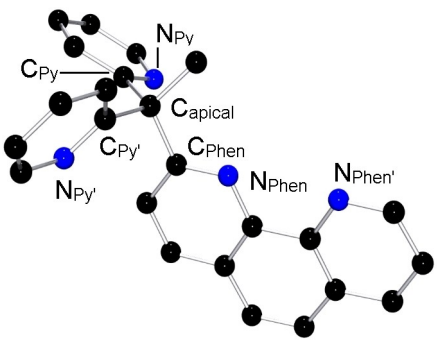

Figure 1. Molecular structure of ligand **L** in the solid state. Hydrogen atoms and the other independent molecule are omitted for clarity. Black = carbon, blue = nitrogen.

© 2020 The Authors. Published by Wiley-VCH Verlag GmbH & Co. KGaA

Table 1. Selected bond lengths and angles for the two ligand molecules **L** and **L′** in the asymmetric unit.

	L	L′
Bond lengths [Å]		
C_{Py}–C_{apical}	1.528(2)	1.538(3)
C_{Py}–C_{apical}	1.537(3)	1.535(3)
C_{Phen}–C_{apical}	1.537(3)	1.541(3)
Bond angles [°]		
N_{Phen}–C–C_{apical}	116.7(2)	117.4(2)
N_{Py}–C–C_{apical}	116.0(2)	116.3(2)
$N_{Py'}$–C–C_{apical}	114.5(2)	113.8(2)
Distances [Å]		
N_{Phen}–$N_{Phen'}$	2.746(2)	2.777(2)
Dihedral angles [°]		
N_{Phen}–C–C–$N_{Phen'}$	2.5(2)	−5.2(3)

obtained by reaction of **L** with $Fe(OTf)_2 \cdot 2MeCN$ and $[Fe(MeCN)_6](BF_4)_2$ in MeCN, respectively.

The structures of the two complex cations are almost identical (Figure 2, Table 2). Both exhibit a shortened Fe–N_{Phen} bond (1.904 Å and 1.909 Å) and an elongated Fe–$N_{Phen'}$ bond (2.016 Å and 2.022 Å) compared to the other Fe–N bonds. This phenomenon is caused by the rigidity of the phenanthrolinyl unit. In comparison, the literature-known complex $[Fe^{II}(MeCPy_2BiPy)(MeCN)_2](OTf)_2$ (**RC**), which has a more flexible bipyridinyl instead of the phenanthrolinyl unit, shows similar behavior but the elongation is with 1.995 Å less distinct.[6] The Fe–$N_{Phen'}$ bond in **C1** and **C2** is longer than 2.0 Å but the average bond lengths are 1.958 Å and 1.959 Å, respectively. This structural feature indicates that the complexes are low spin species.

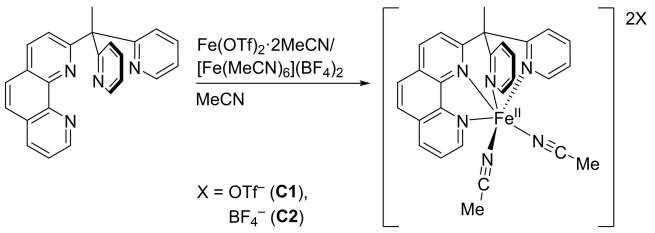

Scheme 3. Synthesis of complexes **C1** and **C2**.

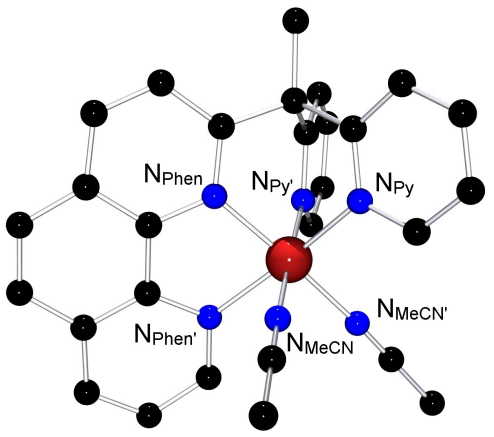

Figure 2. Molecular structure of the cation $[Fe(MeCPy_2Phen)(MeCN)_2]^{2+}$ in the solid state in crystals of **C1**. Hydrogen atoms and anions are omitted for clarity. Black = carbon, blue = nitrogen, scarlet = iron.

Table 2. Selected bond lengths and angles for **C1**, **C2** and reference complex **RC**.

	C1	C2	RC[6] (Phen = BiPy)
Bond lengths [Å]			
Fe–N_{Py}	1.965(2)	1.967(2)	1.969(2)
Fe–$N_{Py'}$	1.955(2)	1.955(2)	1.951(2)
Fe–N_{Phen}	1.904(2)	1.909(2)	1.905(2)
Fe–$N_{Phen'}$	2.016(2)	2.022(2)	1.995(2)
Fe–N_{MeCN}	1.961(1)	1.957(2)	1.950(2)
Fe–$N_{MeCN'}$	1.944(2)	1.944(2)	1.951(2)
Ø Fe–N	1.958	1.959	1.954
Distances [Å]			
N_{Phen}–$N_{Phen'}$	2.564	2.573	
Bond angles [°]			
Fe–N–CMe	175.8(2)	175.7(2)	
Fe–N–CMe′	171.9(2)	172.3(2)	
Structure parameters			
CSM *S*(OC-6)	0.8	0.7	0.6
CSM *S*(TPR-6)	12.6	12.1	13.1

Continuous Shape Measure (CSM) Calculations[22] indicate an ideally octahedrally coordinated Fe ion due to low *S*(OC-6) values (ideal octahedron *S*(OC-6) = 0) and high *S*(TPR-6) values (ideal trigonal prism *S*(TPR-6) = 0). In comparison the *S*(OC-6) value is slightly lower and the *S*(TPR-6) value is a bit higher for the literature known complex **RC** where the coordination is slightly closer to ideal octahedral. This observation is reasonable because the bipyridinyl unit of **RC** is less rigid than the phenanthrolinyl unit of **C1** and **C2**.

Cyclic voltammograms of **C1** (in MeCN) were measured at different scan rates (20–200 mV/s) and are presented in Figure 3.

For better comparison the potential of all measurements is referred to the ferrocene/ferrocenium couple (Fc/Fc^+). The ΔE of 0.064 V indicates a reversible electron transfer as well as the only small shifts of E^{ox} and E^{red} for different sweep rates. The redox potential is located at $E_{1/2} = 0.84$ V. Together this suggests a reversible one electron transfer of a Fe^{II}/Fe^{III} couple. The structurally comparable complex **RC** was previously shown to reveal a comparable redox potential at $E_{1/2} = 0.89$ V.[6] So the reaction of **C1** with mCPBA should be easier.

In the comparison of the UV/Vis absorptions of **C1** and **RC** both show characteristic absorptions in the range of 330 nm up to 600 nm (Figure 4).

C1 shows three absorption maxima whereas **RC** shows only two. These are characteristic features for phenanthrolinyl and bipyridinyl moieties.[23] The extinction coefficients are

© 2020 The Authors. Published by Wiley-VCH Verlag GmbH & Co. KGaA

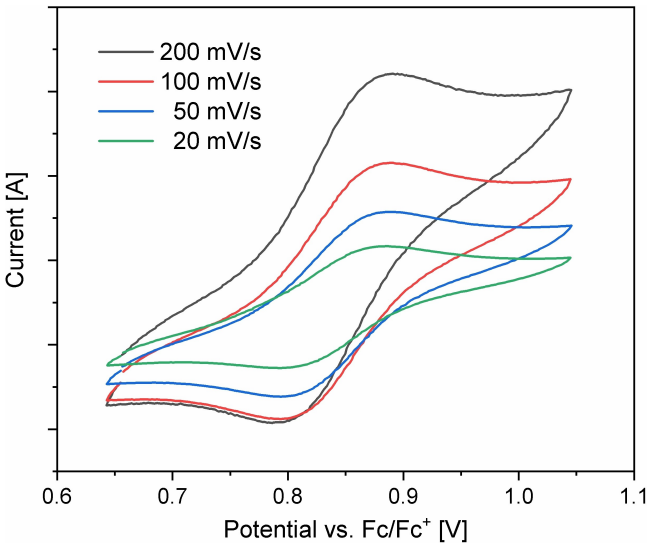

Figure 3. Cyclic voltammogram for **C1** at different sweep rates in MeCN.

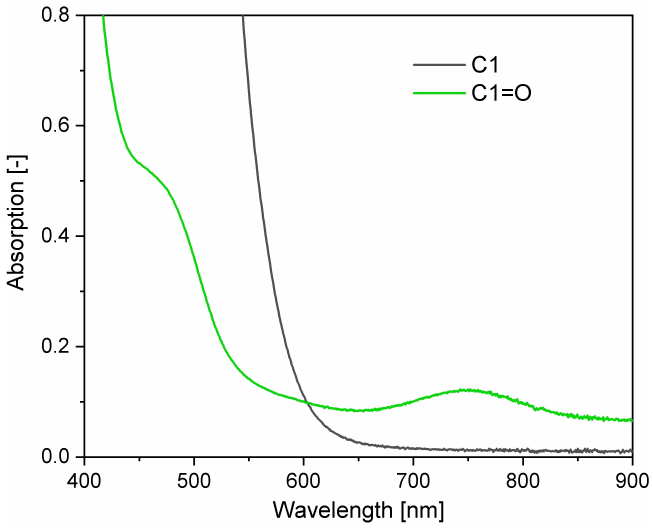

Figure 5. UV/Vis spectra of the precursor **C1** (black, 2.4 mM) and Fe (IV)oxo complex **C1=O** (green, ≤2 mM) in MeCN at room temperature.

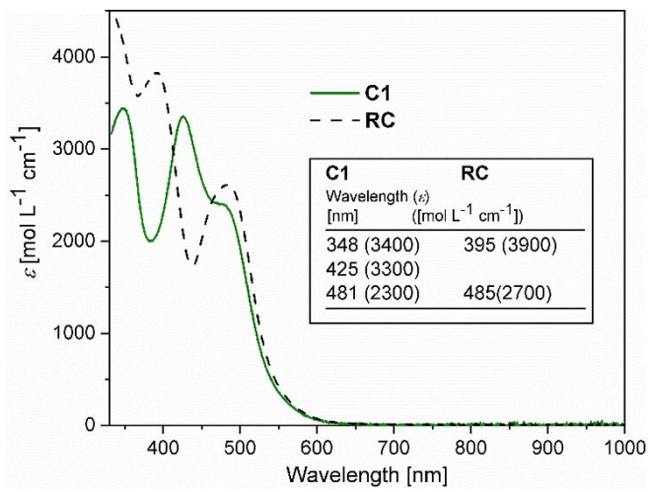

Figure 4. UV/Vis spectra of **C1** (green, strait) and **RC** (black, dashed) in MeCN at room temperature. The maxima and the corresponding molar extinction coefficients are given in the inset table.

quite similar for both complexes. The position of the absorption maxima is blue-shifted for **C1** compared to **RC**.

2.2 Synthesis and Characterization of the High-valent Iron-oxo Species

2.2.1 UV/Vis Measurements

The precursor complex **C1** (orange solution) has no UV/Vis bands around 700 nm (Figure 5), which is a typical area for Fe (IV)oxo bands.[9] Addition of 1.5 eq. of mCPBA leads to a spectrum with a new band at 752 nm indicating the formation of an Fe(IV)oxo species **C1=O** (Figure 5). The solution has a pale green color. The band at 752 nm decays within 10 min ($t_{1/2} \approx 5$ min). Parallel to this band, shoulders at 460 nm and 568 nm are increasing which is assumed to be the formation of one or more decomposition products. A unimolecular reaction can be assumed due to the isosbestic point at 665 nm (Figure 6).

The decay does not follow exponential kinetics and multiple decay pathways might be possible. For the decom-

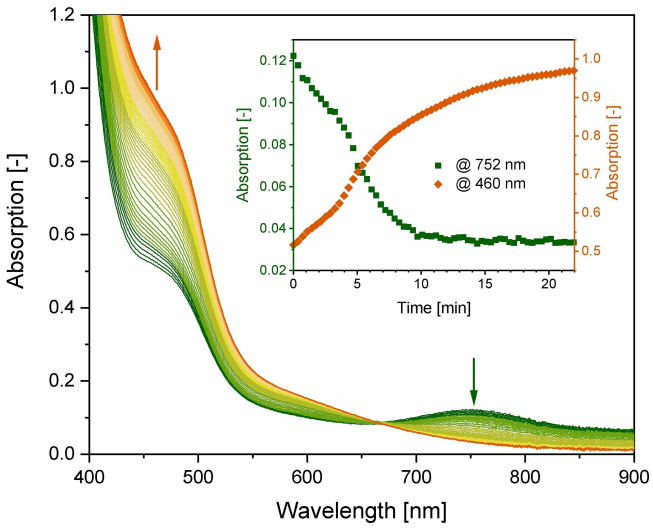

Figure 6. UV/Vis spectra of the decay of the Fe(IV)oxo species (752 nm) and formation of a decomposition product (460 nm) in MeCN at room temperature. Inset: Time-resolved development of the decay (green) and the decomposition product formation (orange).

© 2020 The Authors. Published by Wiley-VCH Verlag GmbH & Co. KGaA

position product shoulder at 460 nm no saturation could be observed.

2.2.2 Stopped-Flow Measurements

For closer investigation of the formation and the subsequent decay of iron-oxo species, stopped flow measurements were performed at different temperatures (−20 °C to 20 °C). Three different observations can be made from these measurements (see Figures S1–S2 in SI). First, the iron-oxo species forms in higher yields at lower temperatures (here: −20 °C). Second, the formation gets slower with decreasing temperature (0.42 min at 20 °C compared to 6 min at −20 °C). Third, the subsequent decay is also slower for lower temperatures. Furthermore, a formation of the iron-oxo species at −40 °C was not observed.

2.2.3 Recovery of the Iron-oxo species

Subsequently, it was tested if **C1=O** could be recovered by adding mCPBA again. For this purpose, a UV/Vis setup with fast scans and a cuvette where the solution could be stirred was chosen. Every 15 min 1 eq. of fresh mCPBA solution was added to the mixture. The experiment was performed under aerobic conditions. Following the time-resolved development of the iron-oxo band at 752 nm reveals that the species could be recovered after all five times of mCPBA addition (Figure 7).

Interestingly the formation and the decay of the iron-oxo species both seem to be faster for the later additions as the band rises and falls faster. It is also worth noting that the maximum absorption of this band is high for the first addition, then lower for the second and getting higher again upwards to the fifth addition. It also has to be taken into account that a decay species is formed with an absorption around 0.12 at 752 nm and that is overlapping with the iron-oxo band. From the second to the fifth addition iron-oxo species is likely formed out of the decay species rather than **C1** because this was consumed at the first addition. Furthermore, the mixture is diluted due to the additions of mCPBA solution. The volume after the fifth addition was 117 % of the starting volume. In total this experiment shows that the iron-oxo species could be obtained not only once but several times also from the decay species. This is an important hint for this species being adapted for catalysis since the catalytically active species needs to be formed for every catalytic cycle. Due to the overlap with the decay product band no precise statement considering the completeness of the individual formations of the iron-oxo species could be made.

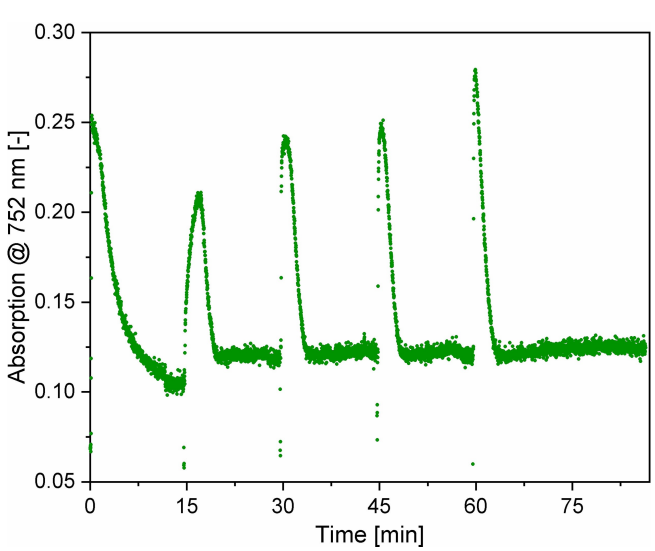

Figure 7. Time resolved development of the absorption at 752 nm with addition of 1 eq. mCPBA (in solution) at 0 min, 15 min, 30 min, 45 min and 60 min.

2.2.4 Mößbauer Measurements

In order to verify the oxidation state and nature of the observed species **C1=O** formed upon treatment with mCPBA, Mößbauer spectroscopy was performed. For this purpose, the complex was dissolved in acetonitrile (Figure 8. Frozen complex solutions were measured at 80 K. Complex **C1** revealed a single low spin Fe(II) system with an isomer shift of 0.42 $mm\,s^{-1}$ along with a quadrupole splitting of 0.51 $mm\,s^{-1}$. Contrary, upon addition of 2 eq. mCPBA to the very same complex solution at −20 °C, a set of two new quadrupole doublets appears with a distribution of 37 % and 63 %, respectively. The minor quadrupole doublet with an isomer shift of 0.04 $mm\,s^{-1}$ close to zero and a corresponding quadrupole splitting of 0.54 $mm\,s^{-1}$ is well in line with the formation of a high-spin Fe(IV)oxo compound and comparable values were previously reported for tetradentate $tpa^{Ph}Fe(IV)O$ ($\delta = 0.09\ mm\,s^{-1}$; $\Delta E_Q = 0.51\ mm\,s^{-1}$; $S = 2$; tpa^{Ph}: tris(5-phenylpyrrole-2-ylmethyl) amine)[24] and other ferryl species.[25,26] In addition, a ferric species ($\delta = 0.48\ mm\,s^{-1}$; $\Delta E_Q = 1.91\ mm\,s^{-1}$) is observed and a similar Mößbauer spectrum upon Fe(IV)oxo formation was previously reported by Nordlander and colleagues and assigned to an oxo-bridged iron dimer impurity.[27] We assume that the observed Fe(III) species results from the decomposition of the intermediate Fe(IV)oxo compound. To support our assumption, the experiment was repeated under otherwise identical conditions but for an extended period of time. Notably, while no ferryl species can be observed, the ferric species is now the only visible product showing identical isomer shifts and quadrupole couplings as before. We thus assume that upon reaction with mCPBA, complex **C1** is being oxidized to form ferryl–**C1** (**C1=O**) that further decomposes to afford a stable ferric complex.

© 2020 The Authors. Published by Wiley-VCH Verlag GmbH & Co. KGaA

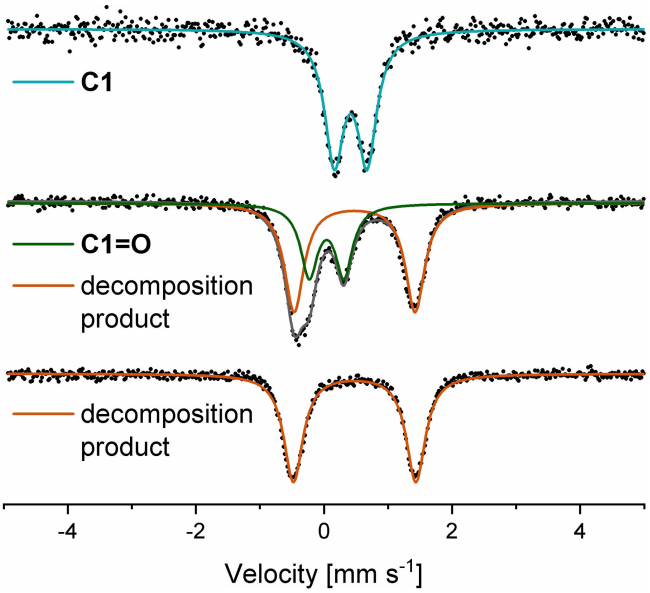

Figure 8. Mößbauer spectra of: top: **C1** (blue, $\delta = 0.42\ mm\,s^{-1}$, $\Delta E_Q = 0.51\ mm\,s^{-1}$) as frozen MeCN solution, middle: reaction solution of **C1** with mCPBA directly after addition at −20 °C as frozen MeCN solution showing **C1=O** species (green, $\delta = 0.04\ mm\,s^{-1}$, $\Delta E_Q = 0.54\ mm\,s^{-1}$) and decomposition product (orange, $\delta = 0.48\ mm\,s^{-1}$, $\Delta E_Q = 1.89\ mm\,s^{-1}$) and bottom: reaction solution after 4 h at −20 °C showing only decomposition product (orange, $\delta = 0.48\ mm\,s^{-1}$, $\Delta E_Q = 1.91\ mm\,s^{-1}$).

2.2.5 CSI-mass Spectrometry Experiment

C1=O was analyzed by high resolution cryospray-ionisation mass spectrometry (CSI-MS) at −20 °C in MeCN (Figure 9). The obtained MS perfectly match the calculated isotope distribution pattern of $[Fe^{IV}(MeCPy_2Phen)O]^{2+}$ with the main signal centered at 217 *m/z* and further supports a reaction of **C1** with mCPBA to an iron-oxo species (Scheme 4).

Two other species could be identified by means of the isotopic distribution pattern in the CSI-MS spectrum (Figure S5 in SI). The first one is $C_{31}H_{22}ClFeN_4O_3^{+}$ with the main signal centred at 589 *m/z* which would fit an adduct of the complex and mCPBA. This may be formulated as $[Fe^{II}(MeCPy_2Phen)(3\text{-}Cl\text{–}(C_6H_4)\text{–}CO_3)]^{+}$ or $[Fe^{IV}(MeCPy_2Phen)(3\text{-}Cl\text{–}(C_6H_4)\text{–}CO_2)O]^{+}$ (Figure S6, Scheme S1 in SI). Similar motives for iron(III)/iron(V) complexes are also discussed in the literature as intermediates for generating iron-oxo complexes with peracids.[28] The second species $C_{62}H_{44}Cl_2Fe_2N_8O_5^{2+}$ could be a bridged species with two complexes connected by mCPBA or 3-chlorobenzoic acid. Possible formulas for this would be $[Fe^{II}(MeCPy_2Phen)(3\text{-}Cl\text{–}(C_6H_4)\text{–}CO_3)\text{–}(3\text{-}Cl\text{–}(C_6H_4)\text{–}CO_2)\text{–}Fe^{II}(MeCPy_2Phen)]^{2+}$ or $[Fe^{IV}(MeCPy_2Phen)O(3\text{-}Cl\text{–}(C_6H_4)\text{–}CO_2)\text{–}O_2\text{–}Fe^{II}(MeCPy_2Phen)(3\text{-}Cl\text{–}(C_6H_4)\text{–}CO_2]^{2+}$ (Figure S7, Scheme S2 in SI).

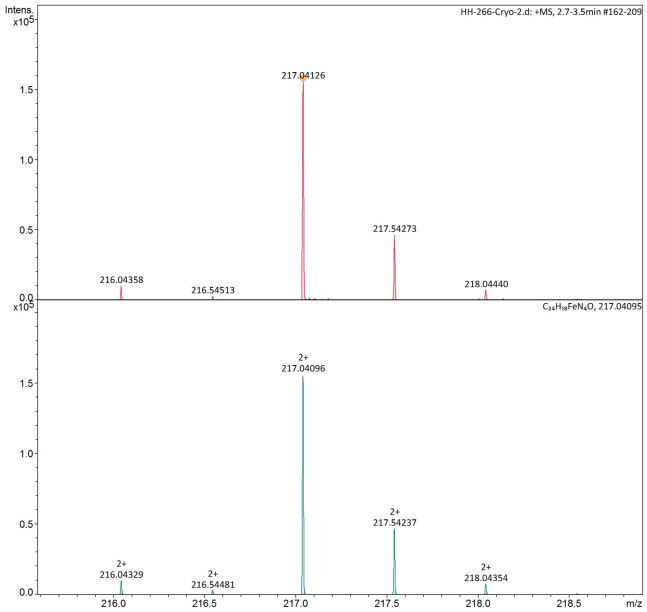

Figure 9. Experimental (top) and calculated (bottom) isotope distribution pattern for $[Fe^{IV}(MeCPy_2Phen)O]^{2+}$.

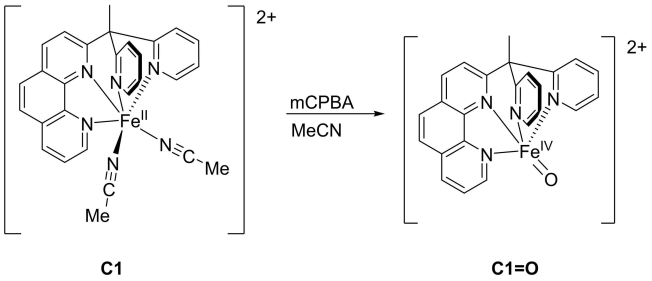

Scheme 4. Reaction of **C1** with mCPBA to $[Fe^{IV}(MeCPy_2Phen)O]^{2+}$ (**C1=O**).

2.3 Catalytic Oxidation of C–H Bonds

The ability of catalytic C–H bond oxidation was tested with cyclohexane as substrate which has relatively strong C–H bonds (C–H BDE = 99.2 kcal/mol; Scheme 5, Table 3).[25,29] To determine whether the oxidation is performed by a metal-based species or not, the alcohol-to-ketone ratio (*A*/*K*) is an important index which gives a first impression on this issue. If, after the initial H atom abstraction, a rapid rebound of the

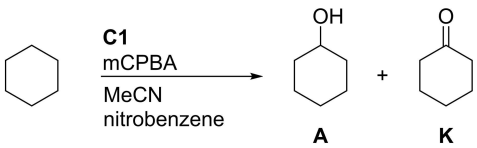

Scheme 5. Catalytic reaction of cyclohexane to cyclohexanol (A) and cyclohexanone (K).

© 2020 The Authors. Published by Wiley-VCH Verlag GmbH & Co. KGaA

Israel Journal of Chemistry

Table 3. Catalytic oxidation of cyclohexane with **C1**.

entry	**C1**:mCPBA:cyclohexane	A/K[a]	efficiency[b]	TON[c]
1	1:10:1000	6.1	53	5
2	1:10:800	5.3	55	6
3	1:10:300	3.2	41	4
4	1:10:100	1.7	25	3
5	1:20:1000	4.0	45	9
6	1:20:800	3.6	44	9
7	1:20:300	1.9	32	7
8	1:20:100	0.9	20	4
9	1:10:1000, air	4.7	61	6

[a] A/K = cyclohexanol/cyclohexanone. [b] efficiency = ((cyclohexanol + cyclohexanone)/mCPBA) · 100. [c] TON = (cyclohexanol + cyclohexanone)/**C1** (all in molar amounts).

carbon centered radical to the now present Fe–OH species is happening, the alcohol is the most favored product.[1] In contrast, a longer living radical usually forms equal amounts of alcohol and ketone ($A/K \approx 1$).

We varied the amount of substrate (100 to 1000 eq.) as well as the amount of oxidizing agent mCPBA (10 or 20 eq.) (Table 3 and Figures 10–12).

For the higher substrate ratios, a high A/K ratio of 6.1 and 4.0 was observed, respectively. This is well above one and is a first hint for a metal-based oxidative species. For lower substrate ratios, the A/K ratio goes down and is close to one, indicating side reactions (Figure 10). These observations are in good agreement with the results of Chen *et al.* for **RC**.[6] They achieved slightly higher A/K ratios of 7.5 and 4.8, respectively.

Additional to these experiments, the reactions with the 1:10:1000 ratio were repeated under aerobic conditions. In this case the A/K ratio was 4.7 instead of 6.1. This is in

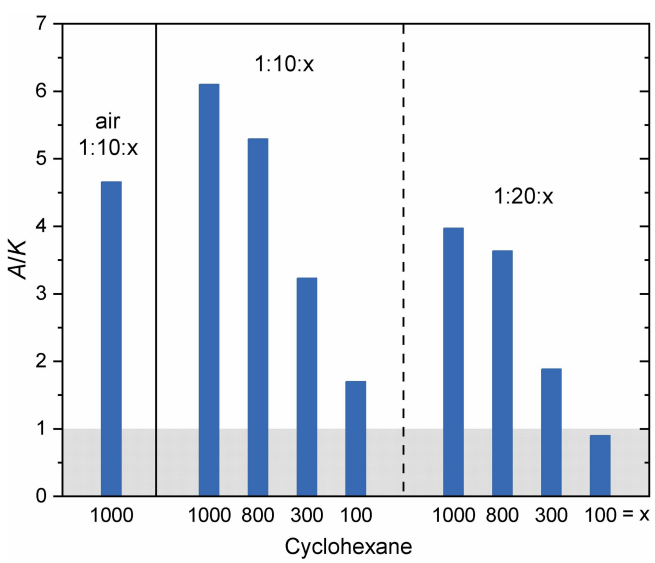

Figure 10. Alcohole-to-ketone ratios (A/K) of catalytic cyclohexane oxidations for different substrate ratios x.

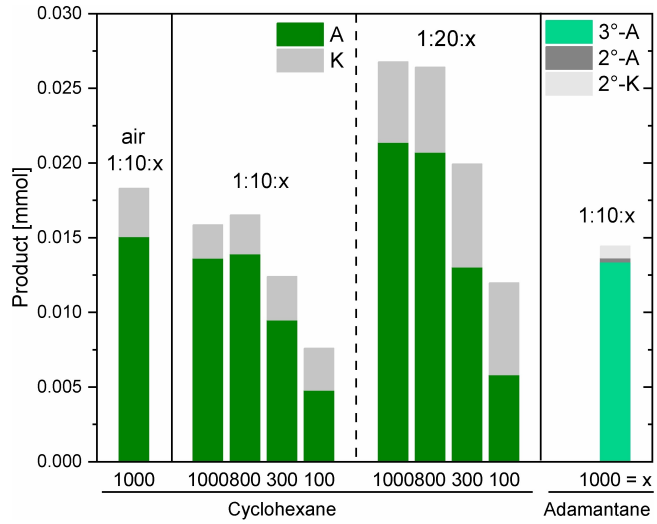

Figure 11. Molar amounts of cyclohexanol (A) & cyclohexanone (K; left) and 1-adamantanol (3°-A), 2-adamantanol (2°-A) & 2-adamantanone (2°-K; right) for different substrate ratios x.

agreement with the literature because the uncontrolled incorporation of molecular oxygen in a non metal-based mechanism leads to the ketone product.[11]

Due to the fact that the oxidant in these reactions is the limiting compound for the maximum yield, it is important to know how much product could be obtained compared with the amount of oxidant used. In this case the efficiency describes this ratio. If the efficiency would be 100% every molecule of oxidant would lead to a desired product molecule. Here, the efficiency of the oxidant mCPBA is with up to 55 in a medium range (Figure 12). For **RC** the efficiency is reported to be higher in a range of 48 (1:10:100) up to 90% (1:10:1000).[6] A reason for this could be that **RC** ($t_{1/2} \approx 30$ min)[6] is stable for a longer period at room temperature than **C1** ($t_{1/2} \approx 5$ min). Turnover numbers (TON) of more than one show that this reaction takes place catalytically since one complex is performing 6 and 9 catalytic cycles, respectively. It is notable that for the double equivalents of mCPBA the TON is also almost doubled. Efficiency and TON both decrease with decreasing amount of cyclohexane used. For the reactions with higher amounts of substrate the oxidation seems to be metal-based.

For the reactions under aerobic conditions TON and efficiency are higher but this might be caused by side reactions with uncontrolled incorporation of molecular oxygen as mentioned before.

One of the next tests for a metal-based oxidant and its strength is the regioselective adamantane oxidation. The latter provides secondary carbon atoms as well as tertiary carbon atoms and can be used to analyze the intermolecular competition of the possible oxidation reactions (Scheme 6). It is expected that the weaker tertiary C–H bond is more likely oxidized. The results are summarized in Table 4 and Figures 11–12.

© 2020 The Authors. Published by Wiley-VCH Verlag GmbH & Co. KGaA

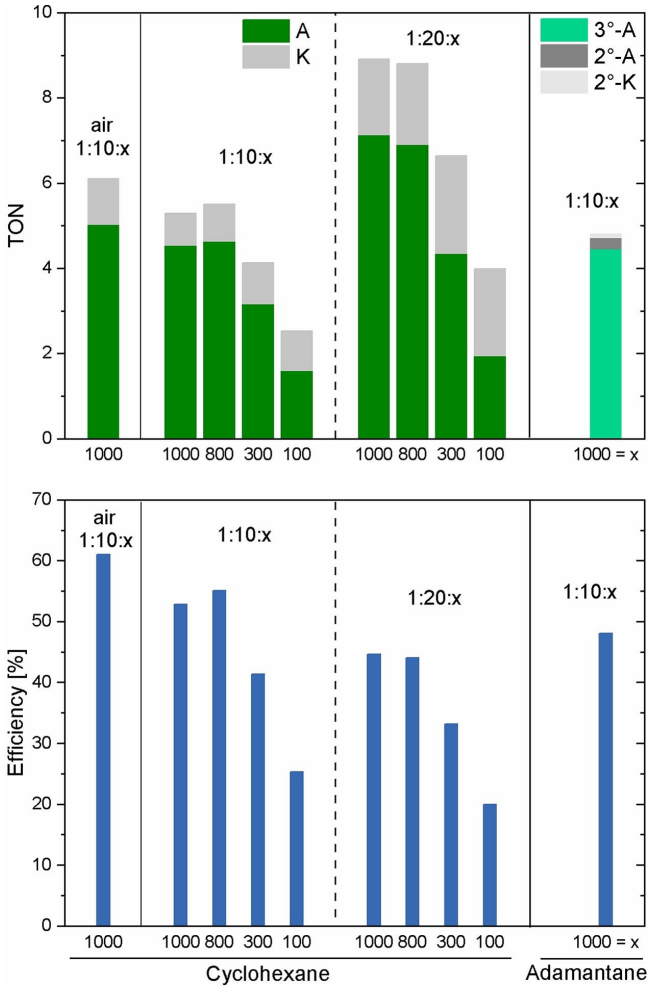

Figure 12. TON for production of cyclohexanol (A) & cyclohexanone (K; left) and 1-adamamantanol (3°-A), 2-adamantanol (2°-A) & 2-adamantanone (2°-K; right) (top) and total efficiency (bottom) for the catalytic oxidation of cyclohexane and adamantane in this work.

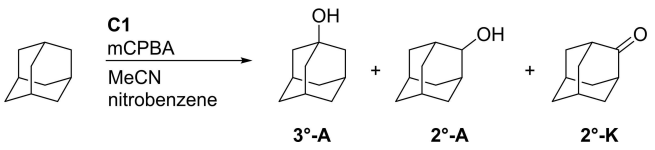

Scheme 6. Catalytic reaction of adamantane to 1-adamatanol (3°-A), 2-adamantanol (2°-A) & 2-adamantanone (2°-K).

Table 4. Catalytic oxidation of adamantane with **C1**.

entry	**C1**:mCPBA:cyclohexane	3°/2°[a]	efficiency[b]	TON[c]
1	1:10:1000	38	48	5

[a] 3°/2° = 3x (1-adamantanol/(2-adamantanol + 2-adamantanone)). [b] efficiency = ((1-adamantanol + 2-adamantanole + 2-adamantanone)/mCPBA)·100. [c] TON = (1-adamantanol + 2-adamantanole + 2-adamantanone)/**C1** (all in molar amounts).

With a tertiary to secondary product ratio (3°/2°) of 38 a clear preference for the tertiary product 1-adamantanol was found. Contrary to the *A*/*K* ratio, the secondary product ration of 3°/2° is nearly independent of the applied substrate amount. For this reason, only one substrate ratio (1 : 10 : 1000) was investigated more closely. Efficiency and TON are in the same range as for the corresponding reactions with cyclohexane as substrate.

Compared to the structurally similar literature known complex **RC** (*A*/*K* = 7.5 and 4.8 [1:x:1000], 3°/2° = 45)[6] the values obtained in this study are slightly lower due to the less stable Fe(IV)oxo species, but still show the same trend. Additionally, the reactions at aerobic conditions are possible. Although indicating slightly more side reactions they still show reasonable results. With regard to the original proposition, that a more rigid coordination increases the catalytic activity, we found that the reverse is true.

3. Conclusion

In summary we presented an iron(II) complex which is stabilized by a tetradentate *N*-donor ligand. This complex enables two *cis*-labile coordination sites which allows oxidation with mCPBA resulting in a Fe(IV)oxo species. This species could be identified by UV/Vis spectroscopy, CSI-MS and Mößbauer measurements. The latter highlight the Fe(IV) oxo species as high-spin species. Furthermore, oxidation catalysis experiments were performed with cyclohexane and adamantane as substrates giving first hints that a metal-based species is the oxidant which we propose to be the Fe(IV)oxo species. These experiments were performed at room temperature which shows that this type of oxidation reactions is possible at mild reaction conditions. This is another step in the direction of sustainable chemistry inspired by the mild reaction conditions of natural enzymes.

4. Experimental Section

4.1 General Remarks

All chemicals and reagents were obtained from commercial sources and were used without further purification unless noted otherwise. 2,2′-(ethane-1,1-diyl)dipyridine, $Fe(OTf)_2 \cdot 2MeCN$, $[Fe(MeCN)_6](BF_4)_2$ and **RC** were synthesized following literature protocols.[6,30] Solvents were dried according to the literature.[31] All compounds were synthesized under nitrogen atmosphere using Schlenk technique or an inert-gas glovebox.

Nuclear magnetic resonance (NMR) spectra were recorded on a Bruker Avance II 400 or Bruker Avance III HD 400 nuclear resonance spectrometer. The signals were calibrated to the residual proton signals of the deuterated solvent.

FT-IR spectra were recorded on a Shimadzu IRTracer 100 using a CsI beam splitter in combination with an ATR unit

© 2020 The Authors. Published by Wiley-VCH Verlag GmbH & Co. KGaA

(Quest model from Specac utilising a robust monolithic crystalline diamond) in a resolution of 2 cm^{-1}.

UV/Vis spectra were measured at ambient temperature with a Cary 60 UV/Vis spectrometer from Agilent Technologies using quartz cuvettes (Hellma, QS, 1 cm). The detection of the iron-oxo species was done according to a protocol of Chen *et al.*[6] Therefore, the iron(II)complex **C1** (4.6 mg 0.006 mmol) was dissolved in MeCN (2.5 mL). 500 µL of a solution of mCPBA (6.2 mg, 0.009 mmol) in MeCN (3 mL) was added to the mixture via a Hamilton syringe and UV/Vis spectra of the resulting iron species were measured.

UV/Vis measurements with stirring for the repeated mCPBA addition were performed with an *Avantes* AvaSpec-ULS2048 CCD-Spectrometer and an *Avantes* AvaLight-DH-S-BAL light source. The measurements were done in *Hellma* QS screw-cap cuvettes with an optical path length of 1 cm. The cuvette holder was connected to lamp and spectrometer via *Avantes* FC-UV200-2 optical fibres.

The stopped-flow measurements were performed with a HI-TECH Scientific SF-61SX2 device with a charge-coupled device (CCD) photodiode array detector. The optical pathlength of the quartz glass cuvette was 1 cm and the mixing time of the two initial solutions (3 mM) was 2 ms. A xenon arc lamp was used as light source. The experiments were performed by mixing two solutions of mCPBA (10.2 mg, 0.06 mmol) in MeCN (20 mL) and **C1** (23.9 mg, 0.03 mmol) in MeCN (10 mL). Both the oxidizing reagent and the precursor complex were transferred as 3 mM solutions in gas-tight Luer Lock syringes. Both solutions were mixed equimolar during the measurement resulting in a 1.5 mM solution of the Fe(IV)oxo compound. The formation was observed at different temperatures from −40 °C to 20 °C.

ESI measurements were performed with an LTQ-Orbitrap XL of ThermoFisher Chemicals (source voltage: 4.49 kV, capillary temperature: 299.54 °C and tube lens voltage: between 110 and 130 V.) or UHR-TOF Bruker Daltonik maXis II (source voltage: 4.50 kV).

Cryospray-ionization mass spectrometry (CSI-MS) measurements were performed on an UHR-TOF Bruker Daltonik maXis II, an ESI-quadrupole time-of-flight (qToF) mass spectrometer capable of a resolution of at least 80.000 FWHM, which was coupled to a Bruker Daltonik Cryospray unit. Detection was in positive ion mode; the source voltage was 3.5 kV. The drying gas (N^2), to achieve solvent removal was held at 0 °C and the spray gas was held at −20 °C. The mass spectrometer was calibrated subsequently to every experiment via direct infusion of a L-proline sodium salt solution, which provided a *m/z* range of singly charged peaks up to 3000 Da in positive ion modes.

Cyclic voltammetry (CV) measurements were performed at room temperature under inert conditions with a Metrohm Autolab Potentiostat PGSTAT 101 using a three-electrode arrangement with a Pt disc working electrode (1 mm diameter), a Pt wire as counter electrode and a Ag wire as reference electrode (pseudo reference). The measurements were performed in MeCN/0.1 mol L^{-1} NBu_4PF_6. Ferrocene was added as an internal standard after the measurements of the sample and all potentials are referenced relative to the Fc/Fc^+ couple. Cyclic voltammograms were measured with 200 mV/s, 100 mV/s, 50 mV/s and 20 mV/s.

The single crystal diffraction data for **L**, **C1** and **C2** are presented in Tables S1 and S2. The single crystal diffraction data were collected on a Stadivari diffractometer of STOE with an Eulerian cradle and Dectris Pilatus3 R 200 K hybrid-pixel detector with GeniX 3D high flux Mo radiation (λ = 0.71073 Å). The temperature was controlled by an Oxford Cryostream 800. Crystals were mounted with grease on glass fibers. Data were collected with X-Area Pilatus and integrated with X-Area Integrate and X-Area Recipe. The absorption correction was performed by Gaussian integration with Stoe X-Red32, afterwards scaling of reflections with X-Area LANA.[32]

The structures were solved by direct methods (XPREP,[33] ShelXS[34] or ShelXT[35]) and refined with ShelXle[36] against F^2 with the full-matrix least-square method (ShelXL).[37] Non-hydrogen atoms were refined with anisotropic displacement parameters. All hydrogen atoms were localized at idealized positions and refined with isotropic displacement parameters. In **C2** it was not possible to model the disordered solvent molecules (CH_3CN) in an adequate manner, and the data set was treated with the SQUEEZE routine as implemented in PLATON.[38] Disorders in **C2** where partly modeled using the DSR[39] tool.

Full crystallographic data have been deposited with the Cambridge Crystallographic Data Centre as supplementary no. CCDC – 1980474 for **L**, CCDC – 1980475 for **C1** and CCDC – 1980476 for **C2**. Copies of the data can be obtained free of charge on application to CCDC, 12 Union Road, Cambridge CB2 1EZ, UK (fax: (+44)1223-336-033; e-mail: deposit@ccdc.cam.ac.uk).

Gas chromatographic measurements were performed on a Shimadzu GC2010plus (FS-Supreme 5mS capillary column; 5% phenylmethylpolysiloxane, length: 30 m, diameter: 0.32 mm, film thickness: 0.25 µm, flame ionisation detector). For quantifying the products, calibration curves were made using nitrobenzene as internal standard. For all peaks the retention times were compared to authentic samples.

Zero-field Mößbauer spectra were recorded at 80 K by using a SeeCo constant acceleration spectrometer equipped with a temperature controller maintaining temperatures within ±0.1 K and a ^{57}Co radiation source in a Rh matrix. Isomer shifts are referred to α-Fe metal at room temperature. Data were fit with a sum of Lorentzian quadrupole doublets by using a least-squares routine with WMOSS program.

© 2020 The Authors. Published by Wiley-VCH Verlag GmbH & Co. KGaA

4.2 Synthesis and Characterization

4.2.1 2-(1,1-di(pyridin-2-yl)ethyl)-1,10-phenanthroline (L)

n-BuLi (4 mL, 2.5 mM, 1.5 eq.) was added dropwise to a solution of 2,2′-(ethane-1,1-diyl)dipyridine (1.9 g, 10.0 mmol, 1.0 eq.) in THF (40 mL) at −78 °C. After stirring for 1 h at −78 °C, 2-bromo-1,10-phenanthroline (1.8 g, 7.0 mmol, 0.7 eq.) was added and the solution was heated over 1 h to 70 °C and refluxed for 48 h. After quenching with water (50 mL) the mixture was extracted with DCM (3x50 mL), washed with brine and dried over Na_2SO_4. The solvent was removed under reduced pressure to get the crude product as red oil. Light yellow solid could be obtained by solvation and isolation of the product in warm *n*-hexane (Yield: 1.5 g, 4.2 mmol, 60 %). Suitable crystals for X-ray diffraction were obtained by evaporation of solids in acetone.

^{1}H-NMR (400 MHz, $CDCl_3$) δ = 9.19 (dd, $^3J_{HH}$ = 4.4, $^4J_{HH}$ = 1.8 Hz, 1H, H-17), 8.58 (ddd, $^3J_{HH}$ = 4.8, $^4J_{HH}$ = 1.9, $^4J_{HH}$ = 0.9 Hz, 2H, H-7), 8.22 (dd, $^3J_{HH}$ = 8.1, $^4J_{HH}$ = 1.8 Hz, 1H, H-15), 8.09 (d, $^3J_{HH}$ = 8.5 Hz, 1H, H-10), 7.74 (d, $^4J_{HH}$ = 1.2 Hz, 2H, H-12, H-13), 7.62–7.55 (m, 4H, H-9, H-5 and H-16), 7.24 (d, $^4J_{HH}$ = 1.1 Hz, 2H, H-4), 7.18–7.05 (m, 2H, H-6), 2.66 (s, 3H, H-1) ppm. ^{13}C-NMR (101 MHz, $CDCl_3$) δ = 166.9 (C-3), 165.7 (C-8), 150.7 (C-17), 149.3 (C-7), 146.7 (C-14), 145.1 (C-11), 136.6 (C-5), 136.5 (C-10), 135.6 (C-15), 129.3 (C-18), 127.6 (C-19), 126.9 (C-13), 126.6 (C-12), 125.8 (C-9), 123.8 (C-4), 122.9 (C-16), 121.7(C-6), 61.6 (C-2), 28.1 (C-1) ppm.

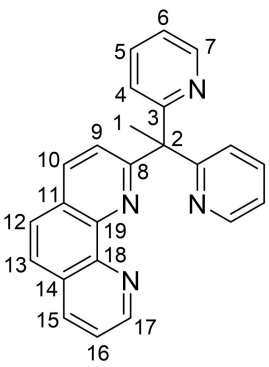

HRMS (EI$^+$): calc. 362.1526 $[C_{24}H_{18}N_4]^+$. Found: 362.1527.

IR $\tilde{\nu}$ [cm^{-1}]: 3855 (vw), 3745 (vw), 2186 (vw), 2161 (vw), 2009 (vw), 1990 (vw), 1735 (vw), 1701 (vw), 1474 (w), 1463 (w), 1441 (w), 1399 (w), 1376 (vw), 1258 (vs), 1221 (m), 1153 (m), 1025 (s), 913 (vw), 870 (w), 845 (w), 833 (w), 810 (m), 780 (m), 771 (m), 765 (m), 755 (w), 750 (w), 738 (w), 731 (w), 681 (w), 666 (w), 655 (w), 635 (vs), 572 (m), 533 (w), 515 (m), 497 (w), 488 (w), 466 (vw), 463 (vw), 447 (vw), 439 (vw), 421 (vw).

4.2.2 [Fe(L)(MeCN)$_2$][(OTf)$_2$] (C1)

To a suspension of $Fe(OTf)_2 \cdot 2MeCN$ (42.0 mg, 0.1 mmol, 1.0 eq.) in MeCN (1 mL) was added a solution of MeC(Py)$_2$Phen (36.0 mg, 0.1 mmol, 1.0 eq.) in MeCN (1 mL). Red crystals were obtained by addition of Et_2O (Yield: 42 mg, 0.05 mmol, 52 %).

IR $\tilde{\nu}$ [cm^{-1}]: 1604 (w), 1454 (w), 1402 (w), 1224 (s), 1156 (s), 1119 (w), 1091 (w), 1062 (w), 1027 (vs), 972 (w), 923 (vw), 869 (vw), 787 (w), 762 (s), 728 (w), 684 (vw), 636 (vs), 609 (m), 572 (m), 516 (m), 472 (vw), 437 (vw), 432 (vw), 415 (w), 409 (vw).

HRMS (ESI$^+$, in MeCN): m/z (%) calc.: 565.04423 (6) $[F_3C_{25}H_{18}N_4O_3{}^{54}FeS]^+$, 567.03956 (100) $[F_3C_{25}H_{18}N_4O_3{}^{56}FeS]^+$, 568.04292 (27) $[F_3{}^{13}C_1{}^{12}C_{24}H^{18}N_4O_3{}^{56}FeS]^+$, 569.03536 (8) $[F_3C_{25}H_{18}N_4O_3{}^{56}Fe^{34}S]^+$ & $[F_3{}^{13}C_2{}^{12}C_{23}H_{18}N_4O_3{}^{56}FeS]^+$. Found: 565.04327 (7), 567.03827 (100), 568.04077 (29), 569.03644 (8).

4.2.3 [Fe(L)(MeCN)$_2$][(BF$_4$)$_2$] (C2)

To a suspension of $[Fe(MeCN)_6](BF_4)_2$ (24.0 mg, 0.05 mmol, 1.0 Eq.) in MeCN (1 mL) was added a solution of MeC(Py)$_2$Phen (16.0 mg, 0.05 mmol, 1.0 Eq.) in MeCN. Red crystals were obtained by addition of Et_2O (18 mg, 0.03 mmol, 54 %).

IR: $\tilde{\nu}$ [cm^{-1}]: 1597 (vw), 1474 (w), 1463 (w), 1441 (w), 1398 (w), 1287 (vw), 1263 (vw), 1047 (vs), 1027 (vs), 867 (w), 846 (w), 809 (w), 779 (w), 763 (m), 738 (w), 730 (w), 680 (w), 666 (m), 577 (vw), 558 (vw), 532 (w), 521 (m), 497 (vw), 478 (vw), 419 (w).

HRMS (ESI$^+$, in MeCN): m/z (%) calc.: 208.04583 (6) $[C_{24}H_{18}N_4{}^{54}Fe]^{2+}$, 208.54751 (2) $[{}^{12}C_{23}{}^{13}C_1H_{18}N_4{}^{54}Fe]^{2+}$, 209.0434 (100) $[C_{24}H_{18}N_4{}^{56}Fe]^{2+}$, 209.54517 (26) $[{}^{12}C_{23}{}^{13}C_1H_{18}N_4{}^{56}Fe]^{2+}$, 210.04685 (3) $[{}^{12}C_{22}{}^{13}C_2H_{18}N_4{}^{56}Fe]^{2+}$. Found: 208.0458 (7), 208.4573 (2), 209.0434 (100), 209.5449 (29), 210.0461 (4).

4.3 C–H Bond Oxidation Reactions

4.3.1 C–H Bond Oxidation Reactions of Cyclohexane by C1

In a typical reaction **C1** (2.4 mg, 0.003 mmol, 1 eq.) and cyclohexane (325 µL, 3 mmol, 1000 eq.) were combined with nitrobenzene (0.015 mmol, internal standard) in 2 mL of dry acetonitrile. To start the reaction mCPBA (0.03 mmol, 10 eq.) in 1 mL of dry acetonitrile was added. It was taken into account that the mCPBA used contained 77 % mCPBA. The reaction mixture was stirred for 2 h at room temperature and stopped with the addition of minimum 25 eq. of PPh_3. To analyze the products 1 mL of the reaction mixture was passed through a short silica column and then submitted to GC

© 2020 The Authors. Published by Wiley-VCH Verlag GmbH & Co. KGaA

analysis. Reactions were carried out at least triplicate. Values shown in this work are averaged.

Reactions at aerobic conditions were performed analogue.

Blind reactions were performed without iron complex as well as $Fe(OTf)_2 \cdot 2MeCN$ instead of **C1**. Without iron complex no products were observed in the GC analysis and use of $Fe(OTf)_2 \cdot 2MeCN$ leads to poorer results as the reactions with **C1** (Table S3 in SI).

4.3.2 C–H Bond Oxidation Reactions of Adamantane by C1

In a typical reaction **C1** (2.4 mg, 0.003 mmol, 1 eq.) and adamantane (409 mg, 3 mmol, 1000 eq.) were combined with nitrobenzene (0.015 mmol, internal standard) in 2 mL of dry acetonitrile. To start the reaction mCPBA (0.03 mmol, 10 eq.) in 1 mL of dry acetonitrile was added. It was taken into account that the mCPBA used contained only 77% mCPBA. The reaction mixture was stirred for 2 h at room temperature and stopped with the addition of minimum 25 eq. of PPh_3. To analyze the products 1 mL of the reaction mixture was passed through a short silica column and then submitted to GC analysis. Reactions were carried out at least triplicate. Values shown in this work are averaged.

Blind reactions were performed without iron complex as well as $Fe(OTf)_2 \cdot 2MeCN$ instead of **C1**. Both leads to poorer results as the reactions with **C1** (Table S4 in SI).

Acknowledgements

Financial support by the Deutsche Forschungsgemeinschaft (SeleCa) and a RWTH ERS SeedFund is acknowledged. U.-P. A. is thankful for financial support by the Deutsche Forschungsgemeinschaft (Emmy Noether grant to U.-P.A., AP242/2-1). This work was supported by the Fraunhofer Internal Programs and Grant No. Attract 097-602175.

References

[1] S. Kal, S. Xu, L. Que, *Angew. Chem. Int. Ed.* **2019**, 10.1002/anie.201906551.
[2] K. Chen, M. Costas, J. Kim, A. K. Tipton, L. Que, *J. Am. Chem. Soc.* **2002**, *124*, 3026.
[3] L. Que, R. Y. N. Ho, *Chem. Rev.* **1996**, *96*, 2607.
[4] a) I. Schlichting, J. Berendzen, K. Chu, A. M. Stock, S. A. Maves, D. E. Benson, R. M. Sweet, D. Ringe, G. A. Petsko, S. G. Sligar, *Science* **2000**, *287*, 1615; b) M. Sono, M. P. Roach, E. D. Coulter, J. H. Dawson, *Chem. Rev.* **1996**, *96*, 2841.
[5] B. J. Wallar, J. D. Lipscomb, *Chem. Rev.* **1996**, *96*, 2625.
[6] L. Chen, X.-J. Su, J. W. Jurss, *Organometallics* **2018**, *37*, 4535.
[7] X. Engelmann, I. Monte-Pérez, K. Ray, *Angew. Chem. Int. Ed.* **2016**, *55*, 7632; *Angew. Chem.*, **2016**, *128*, 7760–7778.
[8] G. Olivo, O. Cussó, M. Borrell, M. Costas, *J. Biol. Inorg. Chem.* **2017**, *22*, 425.
[9] A. R. McDonald, L. Que, *Coord. Chem. Rev.* **2013**, *257*, 414.
[10] M. Costas, M. P. Mehn, M. P. Jensen, L. Que, *Chem. Rev.* **2004**, *104*, 939.
[11] P. Comba, M. Maurer, P. Vadivelu, *Inorg. Chem.* **2009**, *48*, 10389.
[12] A. F. Hollemann, E. Wieberg, N. Wieberg, *Lehrbuch der Anorganischen Chemie*, 91. Aufl., de Gruyter, Berlin, **1985**.
[13] J.-U. Rohde, J.-H. In, M. H. Lim, W. W. Brennessel, M. R. Bukowski, A. Stubna, E. Münck, W. Nam, L. Que, *Science* **2003**, *299*, 1037.
[14] a) K. Chen, L. Q. Jr., *Chem. Commun.* **1999**, 1375; b) K. Chen, L. Que, *J. Am. Chem. Soc.* **2001**, *123*, 6327.
[15] M. H. Lim, J.-U. Rohde, A. Stubna, M. R. Bukowski, M. Costas, R. Y. N. Ho, E. Munck, W. Nam, L. Que, *Proc. Natl. Acad. Sci. USA* **2003**, *100*, 3665.
[16] A. N. Biswas, M. Puri, K. K. Meier, W. N. Oloo, G. T. Rohde, E. L. Bominaar, E. Münck, L. Que, *J. Am. Chem. Soc.* **2015**, *137*, 2428.
[17] J. Yoon, S. A. Wilson, Y. K. Jang, M. S. Seo, K. Nehru, B. Hedman, K. O. Hodgson, E. Bill, E. I. Solomon, W. Nam, *Angew. Chem. Int. Ed.* **2009**, *48*, 1257; *Angew. Chem.* **2009**, *121*, 1283–1286.
[18] S. Hong, Y.-M. Lee, K.-B. Cho, K. Sundaravel, J. Cho, M. J. Kim, W. Shin, W. Nam, *J. Am. Chem. Soc.* **2011**, *133*, 11876.
[19] M. P. Jensen, M. Costas, R. Y. N. Ho, J. Kaizer, A. Mairata i Payeras, E. Münck, L. Que, J.-U. Rohde, A. Stubna, *J. Am. Chem. Soc.* **2005**, *127*, 10512.
[20] J. Bautz, P. Comba, C. Lopez de Laorden, M. Menzel, G. Rajaraman, *Angew. Chem. Int. Ed.* **2007**, *46*, 8067; *Angew. Chem.* **2007**, *119*, 8213–8216.
[21] Q. Teng, H. V. Huynh, *Dalton Trans.* **2017**, *46*, 614.
[22] a) M. Llunell, D. Casanova, J. Ciera, P. Alemany, S. Alvarez, *SHAPE. Continous Shape Measures calculation*, Electronic Structure Group, Universitat de Barcelona, **2013**; b) S. Alvarez, D. Avnir, M. Llunell, M. Pinsky, *New J. Chem.* **2002**, *26*, 996.
[23] a) G. Accorsi, A. Listorti, K. Yoosaf, N. Armaroli, *Chem. Soc. Rev.* **2009**, *38*, 1690; b) M. S. Henry, M. Z. Hoffman, *J. Phys. Chem.* **1979**, *83*, 618.
[24] J. P. Bigi, W. H. Harman, B. Lassalle-Kaiser, D. M. Robles, T. A. Stich, J. Yano, R. D. Britt, C. J. Chang, *J. Am. Chem. Soc.* **2012**, *134*, 1536.
[25] J. Kaizer, E. J. Klinker, N. Y. Oh, J.-U. Rohde, W. J. Song, A. Stubna, J. Kim, E. Münck, W. Nam, L. Que, *J. Am. Chem. Soc.* **2004**, *126*, 472.
[26] K. Cheaib, M. Q. E. Mubarak, K. Sénéchal-David, C. Herrero, R. Guillot, M. Clémancey, J.-M. Latour, S. P. de Visser, J.-P. Mahy, F. Banse, *Angew. Chem. Int. Ed.* **2019**, *58*, 854; *Angew. Chem.* **2019**, *131*, 864–868.
[27] M. Mitra, H. Nimir, S. Demeshko, S. S. Bhat, S. O. Malinkin, M. Haukka, J. Lloret-Fillol, G. C. Lisensky, F. Meyer, A. A. Shteinman, *Inorg. Chem.* **2015**, *54*, 7152.
[28] a) J. Serrano-Plana, W. N. Oloo, L. Acosta-Rueda, K. K. Meier, B. Verdejo, E. García-España, M. G. Basallote, E. Münck, L. Que, A. Company, *J. Am. Chem. Soc.* **2015**, *137*, 15833; b) O. Cussó, J. Serrano-Plana, M. Costas, *ACS Catal.* **2017**, *7*, 5046.
[29] a) M. S. Seo, N. H. Kim, K.-B. Cho, J. E. So, S. K. Park, M. Clémancey, R. Garcia-Serres, J.-M. Latour, S. Shaik, W. Nam, *Chem. Sci.* **2011**, *2*, 1039; b) R. Singh, G. Ganguly, S. O. Malinkin, S. Demeshko, F. Meyer, E. Nordlander, T. K. Paine, *Inorg. Chem.* **2019**, *58*, 1862.
[30] a) N. S. Sommerfeld, J. Gülzow, A. Roller, K. Cseh, M. A. Jakupec, A. Grohmann, M. Galanski, B. K. Keppler, *Eur. J. Inorg. Chem.* **2017**, *2017*, 3115; b) K. S. Hagen, *Inorg. Chem.* **2000**, *39*, 5867; c) B. J. Hathaway, D. G. Holah, A. E. Underhill, *J. Chem. Soc.* **1962**, *0*, 2444.

© 2020 The Authors. Published by Wiley-VCH Verlag GmbH & Co. KGaA

[31] J. Leonard, B. Lygo, G. Procter, *Praxis der organischen Chemie. Ein Handbuch*, VCH, Weinheim, **1996**.
[32] a) X-Area Recipe 1.33.0.0, **2015**, STOE; b) X-Area Integrate 1.71.0.0, **2016**, STOE; c) X-Area Pilatus3_SV 1.31.131.0, **2017**, STOE; d) X-Area LANA 1.71. 4.0, **2017**, STOE.
[33] Bruker, *XPREP*, Bruker AXS Inc., Madison, Wisconsin, USA, **2007**.
[34] G. M. Sheldrick, *Acta Crystallogr. Sect. A* **2008**, *64*, 112.
[35] G. M. Sheldrick, *Acta Crystallogr. Sect. A* **2015**, *71*, 3.
[36] C. B. Hübschle, G. M. Sheldrick, B. Dittrich, *J. Appl. Crystallogr.* **2011**, *44*, 1281.
[37] G. M. Sheldrick, *Acta Crystallogr. Sect. C* **2015**, *71*, 3.
[38] a) A. L. Spek, *Acta Crystallogr. Sect. D* **2009**, *65*, 148; b) A. L. Spek, *PLATON. A Multipurpose Crystallographic Tool*, Utrecht University, Utrecht (The Netherlands), **2008**.
[39] a) D. Kratzert, I. Krossing, *J. Appl. Crystallogr.* **2018**, *51*, 928; b) D. Kratzert, J. J. Holstein, I. Krossing, *J. Appl. Crystallogr.* **2015**, *48*, 933.

Manuscript received: February 7, 2020
Revised manuscript received: March 9, 2020
Version of record online: ■■, ■■

© 2020 The Authors. Published by Wiley-VCH Verlag GmbH & Co. KGaA

FULL PAPER

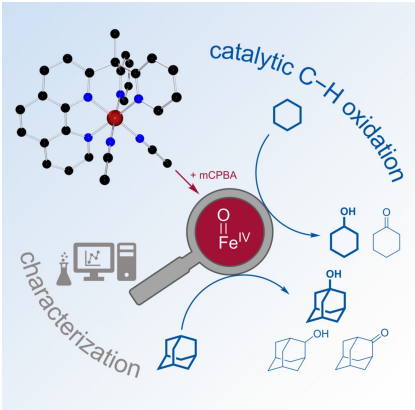

*H. M. Hüppe, K. Keisers, F. Fink, S. D. Mürtz, Dr. A. Hoffmann, L. Iffland, Prof. Dr. U.-P. Apfel, Prof. Dr. S. Herres-Pawlis**

1 – 13

Catalytically Active Iron(IV)oxo Species Based on a Bis(pyridinyl) phenanthrolinylmethane